nature communications

Article

https://doi.org/10.1038/s41467-025-57720-x

# Sustainable bioactive hydrogels for organic contaminant elimination in wastewater

Received: 23 August 2024

Accepted: 27 February 2025

Published online: 13 March 2025

Check for updates

Jinlong Zhang[1], Jason C. White[2], Jinglei He[1], Xuefeng Yu[1], Chuanhao Yan[1], Liang Dong[1], Shu Tao[1] & Xilong Wang[1]

Immobilized enzyme bioremediation is a promising technique for eliminating pollutants to alleviate water scarcity pressure but is severely hindered by poor enzymatic activity and stability. An effective charge-assisted H-bonding approach is developed to achieve high laccase loading and enzymatic activity on bio(cellulose)-based hydrogels. Notably, this strategy can be readily extended to lipase and catalase. The bio-based hydrogels are synthesized by grafting deoxyribonucleic acid onto the cellulose backbone through a one-step structural regulation, achieving high mechanical strength, enzyme loading and contaminant capture for degradation. The biocompatible laccase-immobilized hydrogels exhibit significant removal and degradation performance for diverse organic micropollutants, including parent and substituted polycyclic aromatic hydrocarbons, per- and polyfluoroalkyl substances, antibiotics and organic dyes. Further testing focused on parent and substituted polycyclic aromatic hydrocarbons shows minimal influence of various co-existing interfering substances on performance of the laccase-immobilized bioactive hydrogel, with its contaminant removal and degradation efficiency in authentic wastewater being 93.0- and 64.3-fold that of commercial free laccase, respectively. This work provides an effective strategy for sustainable bioremediation of wastewater and other pollutant streams, while simultaneously enabling the development of innovative enzyme catalysts.

Global water scarcity poses a significant obstacle to achieving the United Nations' Sustainable Development Goals[1–3]. Current estimates are that four billion people lack access to fresh surface and groundwater resources at least one month annually, while an estimated 500 million people face year-round water scarcity[4]. A crucial strategy for alleviating water scarcity pressure is the purification and reuse of contaminated wastewater via treatment plants[5]; however, conventional strategies are often ineffective at removing micropollutants[6]. Found at low concentrations (ng/L-μg/L) relative to other pollutants of public concern[7,8], micropollutants are ubiquitous and pose a significant risk to both environmental and human health due to high toxicity (cancer and neurotoxicity), persistence, and strong bioaccumulation potential[9,10]. Therefore, the development of effective and sustainable strategies to effectively eliminate these pollutants from marginal water sources is urgently needed.

To date, conventional wastewater remediation approaches include sorption, flocculation, advanced oxidation, and biodegradation[9,11,12]. Among them, biodegradation, particularly enzyme-catalyzed degradation, exhibits a number of advantages such as low cost, negligible secondary pollution, and the ability to overcome the complex cultivation processes and harsh operating conditions through microbiological degradation[12,13]. However, the sensitive tertiary structure of relevant enzymes may undergo denaturation during harsh remediation conditions, subsequently hampering long-term stability and widespread applicability[14]. In addition, many enzymes of interest function as water-soluble homogeneous degrading agents that require expensive

[1]Laboratory for Earth Surface Processes, College of Urban and Environmental Sciences, Peking University, Beijing, China. [2]The Connecticut Agricultural Experiment Station, New Haven, CT, USA. e-mail: xilong@pku.edu.cn

ultrafiltration systems for analyte recovery. Consequently, most strategies involve disposal after single use, increasing cost and confounding efforts to align with the principles of a circular green economy[15].

Enzyme immobilization technologies can effectively address many of the aforementioned shortcomings by utilizing carrier materials to confine the enzymes within a specific space, thereby safeguarding and potentially enhancing their degradation activity and facilitating enzyme recycling[15]. Recently, a number of enzyme carriers have been synthesized, including carbon nanomaterials (e.g., carbon nanotubes), hydrogels, and metal-organic frameworks[16–19], opening possibilities for green bioremediation of wastewater. Among these materials, hydrogels have generated much interest due to their highly amenable three-dimensional polymer carrier structure and soft matrices for enzyme immobilization, which is a direct function inherent resemblance to natural extracellular matrices known to be suitable for protein retention (allowing enzyme adaptation and structural optimization)[20]. Unfortunately, many current hydrogels for enzyme immobilization rely heavily on synthetic polymers with complex design and synthesis conditions, resulting in high energy consumption and cost, as well as lack of environmental sustainability with regard to ecological risk[20,21]. Consequently, bio-based materials have been attracting increasing research attention. For example, deoxyribonucleic acid (DNA)-based hydrogels have been used for immobilizing enzymes (galactose oxidase, glucose oxidase, and horseradish peroxidase) to increase their enzymatic activity by enhancing diffusion and cascade effects[22,23]. Additionally, effective enzyme-immobilized hydrogels must possess high mechanical strength and micropollutant capture potential as these factors are critical for their practical application[6,24]. However, the construction of hydrogels that demonstrate sustainability, cost-effectiveness, excellent mechanical strength and ability for micropollutant capture remains a formidable challenge.

On this basis, the key to effective pollutant elimination lies in high enzyme loading and the maintenance/optimization of the associated enzymatic activity within the hydrogel[19]. However, reconciling these two factors remains problematic[25] because (1) hydrogels typically possess a limited specific surface area, resulting in low enzyme loading and immobilization[26]; (2) weak forces (electrostatic, hydrophobic, and ordinary H-bond) between the enzyme and hydrogel lead to low stability[27]; (3) stronger interaction forces (such as covalent bonding) between them often significantly change the enzymatic conformation and lead to inactivation[15,27]. Additionally, much of the current research on enzyme immobilization for environmental remediation primarily focuses on a single pollutant or a specific class of chemicals, which greatly limits its application and commercial viability. Furthermore, many of these studies evaluate performance with laboratory-simulated wastewater[28]. However, authentic wastewater has a complex composition containing a diverse range of co-existing substances, including dissolved organic matter (DOM), heavy metals, and other organic pollutants[19]. These factors inevitably influence the effectiveness of micropollutant remediation.

In this work, a simple structural regulation strategy is used to synthesize bio-based hydrogels (Cellulose-DNA) with high enzyme loading/activity and mechanical strength conveyed through the use of a cross-linker to graft DNA onto the cellulose backbone for capturing micropollutants. This effective and scalable enzyme immobilization strategy demonstrates high enzyme loading and activity with laccase, an oxidoreductase enzyme widely utilized for the degradation of pollutants. Mechanistically, Cellulose-DNA hydrogels rely on charge-assisted hydrogen bonding (CAHB), which has an intermediate strength between weak interactions and strong covalent bonds. The laccase-immobilized Cellulose-DNA hydrogels demonstrate significant removal/degradation performance and applicability for three representative micropollutants (i.e., fluoranthene: Flu, 1-Methylfluoranthene: 1-MFlu, 3-Nitrofluoranthene: 3-NFlu), as well as per- and polyfluoroalkyl substances (PFAS), antibiotics, and organic dyes. Importantly, excellent remediation performance for 16 USEPA priority parent polycyclic aromatic hydrocarbons (PAHs, including Flu) and two substituted PAHs (1-MFlu, 3-NFlu) in authentic wastewater is demonstrated. This study provides a theoretical framework for the advancement of enzyme immobilization techniques and presents a viable approach for their application as a highly efficient environmental remediation tool.

## Results

### Synthesis and characterization of Cellulose-DNA hydrogels

Cellulose-DNA hydrogels were synthesized through a simple structural regulation strategy, aiming to simultaneously increase specific surface area and enhance mechanical strength (Fig. 1a). An increase in a cross-linker 1,4-butanediol diglycidyl ether (BDE) concentration from 0 to 1.6 g significantly enhanced the hydrogel compressive strength (up to 1.25 MPa) (Fig. 1b, Supplementary Fig. 1); mechanistically, BDE serves as a bridge connecting cellulose chains and DNA via covalent bonding. However, the Cellulose-DNA hydrogels BET surface area ($S_{BET}$ < 134.5 $m^2/g$, Supplementary Fig. 2) decreased when the concentration exceeded 0.8 g. Field-emission scanning electron microscopy coupled with energy dispersive spectroscopy (FESEM-EDS) images of the Cellulose-DNA hydrogels revealed significantly enhanced porous structure at the optimal BDE dose (0.8 g) compared to those hydrogels without BDE or at higher BDE doses (1.6 g) (Fig. 1c–e). This enhanced porous structure facilitated greater exposure of active sites for enzyme immobilization (Fig. 1b) and potential micropollutant capture by DNA. Specifically, these Cellulose-DNA hydrogels exhibited a specific surface area of 145.9 $m^2/g$, DNA assembly of 485.7 mg/g, compressive strength of 1.12 MPa, and laccase loading capacity of > 937.3 mg/g (Supplementary Table 1, Supplementary Fig. 3). This optimized hydrogel was selected for subsequent evaluation and enzyme immobilization.

FESEM-EDS images of the Cellulose-DNA hydrogels demonstrate relatively uniform elemental distribution of N, P (from DNA) C, and O on the surface (Supplementary Fig. 4). X-ray photoelectron spectroscopy (XPS) analysis clearly shows N and P signals in the Cellulose-DNA hydrogels (Supplementary Fig. 5a). In addition, Fourier transform infrared spectroscopy (FTIR) spectra show two characteristic peaks attributable to the DNA base thymine (1692 $cm^{-1}$) and $PO^{2-}$ (1228 $cm^{-1}$) (Fig. 1f)[29,30]. Moreover, significant enhancement of the C-O-C peak intensity at 1159 $cm^{-1}$ on the FTIR spectra and at 533.8 eV on the O1s XPS spectra of Cellulose-DNA hydrogels were observed compared to that of the DNA-free hydrogels (Fig. 1g)[31,32]. This is attributed to the formation of C-O-C covalent bonds between BDE and -OH groups on the cellulose skeleton, indicating the successful grafting and cross-linking of DNA onto the cellulose skeleton.

Meanwhile, the binding energy for P $2p^{1/2}$ (134.7 eV) and P $2p^{3/2}$ (133.7 eV) peaks on the P 2p spectra of Cellulose-DNA hydrogels remains unchanged compared to that of DNA (Supplementary Fig. 5b)[33]. However, the N-C-O/N-C = O and C-$NH_2$ peaks on the N 1 s spectra left-shifted by 0.7 eV (Fig. 1h), and the signal intensity for the C-$NH_2$ peak on the N 1 s spectra was significantly lower than that on DNA[33,34]. This phenomenon arises from the cross-linking reaction between BDE and the C-$NH_2$ groups on DNA. The above results collectively confirm successful assembly of DNA onto the cellulose skeleton through BDE-mediated crosslinking mediated by covalent bonding with -$NH_2$ groups. In addition, the crystalline structure (2θ: 15.3°, 16.5°) of a portion of cellulose is evident on the X-ray diffraction (XRD) spectra of Cellulose-DNA hydrogels (Fig. 1i).

Interestingly, a comparison of the XRD spectra of Cellulose- and Cellulose-DNA hydrogels shows that the covalent bond formation between cellulose and BDE during DNA assembly partially damaged the cellulose crystalline structure as indicated by the variation of peak position and intensity at 22.6° on the spectra (Fig. 1i). This process may disrupt the H-bonds among cellulose chains[35], leading to significant increases in the specific surface area and mechanical strength from

https://doi.org/10.1038/s41467-025-57720-x

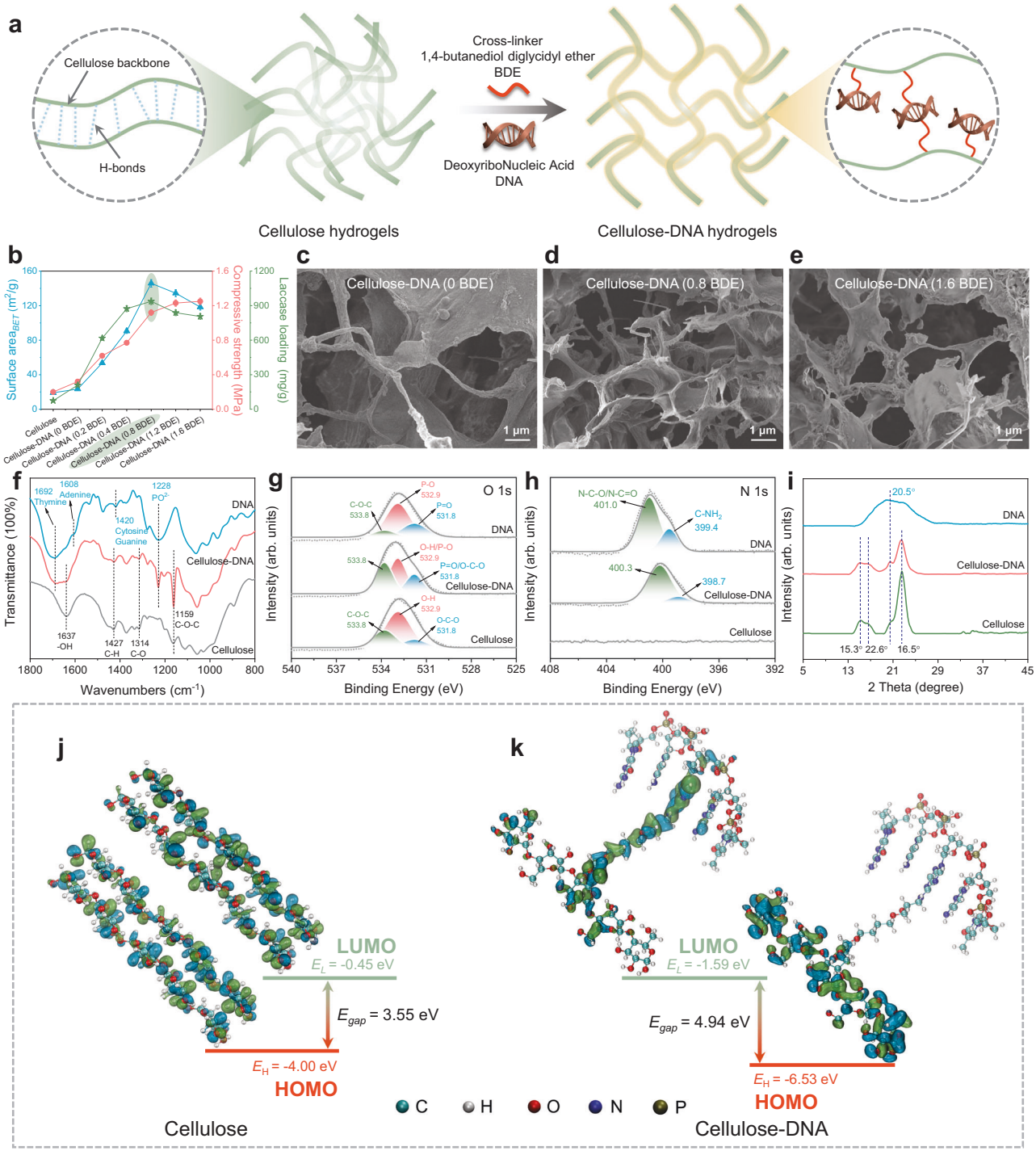


**Fig. 1 | Synthesis and characterization of Cellulose-DNA hydrogels. a** Illustration of the suggested microstructure of the Cellulose-DNA hydrogels by a simple structural regulation strategy. **b** Effect of BDE dose (0-1.6 g) used for DNA assembly on BET specific surface area ($m^2$/g), compressive strength (MPa), and laccase loading (mg/g) of Cellulose-DNA hydrogels. The impact of BDE dose on the immobilized amount of laccase on the Cellulose-DNA hydrogels aligns with the specific surface area data and demonstrates significant potential for laccase immobilization. The green elliptical shadow represents the optimal BDE dose during the synthesis of the Cellulose-DNA hydrogels. FESEM images of the Cellulose-DNA hydrogels synthesized using 0 g BDE (**c**), 0.8 g BDE (**d**), and 1.6 g BDE (**e**). FTIR spectra (**f**), O 1 s (**g**) and N 1 s (**h**) XPS spectra, and XRD patterns (**i**) of the Cellulose hydrogels, Cellulose-DNA hydrogels and DNA. Energy-optimized geometries and the energy gap ($E_{gap} = E_{LUMO} - E_{HOMO}$, eV) of cellulose and cellulose (H-bond interaction) in Cellulose hydrogels (**j**), cellulose and DNA (BDE crosslinking) in Cellulose-DNA hydrogels (**k**) via DFT calculations. Highest occupied molecular orbital: HOMO, lowest unoccupied molecular orbital: LUMO. The molecules with a greater $E_{gap}$, which is an important stability indicator in chemicals, are more stable and less reactive. In (**b**), data are presented as mean ± S.D. from three replicates ($n = 3$).

19.1 $m^2$/g and 0.20 MPa for the Cellulose hydrogels to 145.9 $m^2$/g and 1.12 MPa for the Cellulose-DNA hydrogels, respectively (Fig. 1b). Given that DNA was assembled onto the cellulose skeleton through BDE, which has a longer molecular chain compared to the H-bonds among cellulose chains, DNA assembly likely expanded the inter-chain spacing and thus increased the specific surface area (Fig. 1a).

The covalent bonds between BDE and DNA on the cellulose skeleton are stronger and more stable than the H-bonds among the cellulose

chains; thus, DNA assembly may enhance overall mechanical strength of the hydrogels. The BDE crosslinking interactions between cellulose and DNA in Cellulose-DNA hydrogels was evaluated by DFT calculations using an important stability indicator ($E_{gap} = E_{LUMO} - E_{HOMO}$)[36,37]; this analysis was meant to provide further insight into the underlying molecular mechanisms by which DNA assembly could enhance the mechanical strength of the Cellulose hydrogels and the stability of the H-bond interactions between intra- and inter-molecules of cellulose. The $E_{gap}$ values for the BDE crosslinking (4.94 eV, Fig. 1j, k) from the Cellulose-DNA hydrogels are significantly greater than that of the H-bond from Cellulose hydrogels (3.55 eV), indicating higher stability with DNA inclusion. These experimental and theoretical results consistently demonstrate that the covalent bond connection of DNA to cellulose through BDE served as a bridge during structural regulation, thereby enhancing hydrogel mechanical strength. In addition, the Cellulose-DNA hydrogels exhibited significant micropollutant capture capability (e.g., Flu, Supplementary Fig. 6 and Supplementary Table 2); given the nature of these processes, applicability to additional micropollutants should be possible, subsequently facilitating degradation by the immobilized enzyme.

## Performance of immobilized laccase on Cellulose-DNA hydrogels

Laccase loading on the Cellulose-DNA hydrogel increased with increasing concentration (Supplementary Fig. 7a), with the maximum amount at 2.5 mg/mL (1022 mg/g) of the enzyme. To our knowledge, this loading capacity surpasses that of all materials reported in previous studies (Supplementary Table 1), which can be attributed to the significant specific surface area of the Cellulose-DNA hydrogels. However, enzymatic activity of the immobilized laccase decreased significantly from 203.2 U/g at 2.0 mg/mL laccase to 133.3 U/g at 2.5 mg/mL laccase; this reduction was due to steric hindrance of the excess enzyme that induced conformational changes and inhibited substrate interaction. Therefore, Cellulose-DNA hydrogels immobilized with 937.3 mg/g laccase (2.0 mg/mL laccase) were used in subsequent stability and degradation performance tests. $^1$H nuclear magnetic resonance spectroscopy ($^1$H NMR) and confocal laser scanning microscopy (CLSM) further demonstrated strong laccase immobilization on the Cellulose-DNA hydrogel (Supplementary Fig. 8, Supplementary Table 3). Importantly, the immobilized laccase exhibited a broader pH (3-7) and temperature (15-55 °C) functional range for maintaining enzymatic activity above 80% (Supplementary Fig. 7b, c) relative to the free laccase. In addition, after storage for 30 days, the immobilized laccase maintained an enzymatic activity level as high as 96.1% (Supplementary Fig. 7d), significantly surpassing that of the free laccase (59.1%). Notably, even after undergoing 7 reaction cycles with the substrate 2,2′-azino-bis-(3-ethylbenzothiazoline-6-sulfonic acid) (ABTS), the immobilized laccase maintained excellent enzymatic activity (95.1%) with an immobilized laccase amount of up to 896.1 mg/g (Supplementary Fig. 7e). These findings underscore the significant potential of Cellulose-DNA hydrogels for preserving and stabilizing the laccase enzymatic performance.

Importantly, immobilized enzymes often exhibit inherent disadvantages, including potential coverage of active sites by carriers, which can lead to steric hindrance and a loss of flexibility in ligand binding during degradation[38]. Limitations such as this often reduce substrate affinity of the immobilized relative to the free enzyme (i.e., higher Michaelis constant: $K_m$). A high $K_m$ value indicates that the immobilized enzyme has a low substrate affinity, necessitating a high substrate concentration to attain the maximum reaction rate ($\upsilon_{max}$)[39]. However, the laccase-immobilized Cellulose-DNA hydrogels demonstrate higher affinity ($K_m$: 0.2498 mmol/L) and reaction rate ($\upsilon_{max}$: 0.5315 μmol/(L·min)) towards the substrate ABTS due to analyte capture by DNA as compared to the free enzyme (Supplementary Fig. 7f). This clearly indicates the lack of impact of the aforementioned challenges, which can be attributed to: (1) capture of the substrate ABTS by DNA in the laccase-immobilized hydrogels facilitates analyte mass transfer and diffusion to the active sites on laccase; (2) the structural similarity between Cellulose-DNA hydrogels and natural extracellular matrices provides a protective physical environment that shields enzymes from environmental stresses, which enables dynamic adaptation and optimization of the 3-dimensional conformation and activity of laccase[20,40]; (3) the specific interactions between the Cellulose-DNA hydrogels and laccase ensure stable loading while preserving the functional 3-dimensional conformation (Supplementary Fig. 9). These combined mechanisms resulted in an increased activity of the immobilized laccase, which will facilitate subsequent micropollutant elimination.

## Mechanism of laccase immobilization on Cellulose-DNA hydrogels: CAHB

Both laccase (composed of amino acids, point of zero charge: PZC = 3.72) and Cellulose-DNA hydrogels (composed of polysaccharides and DNA, PZC = 4.11) are hydrophilic and negatively charged at the experimental pH 6.0 (Supplementary Fig. 10). Hence, electrostatic repulsion could hinder the stable and significant immobilization onto the hydrogel, but it is evident that other driving forces must be responsible for their interaction. Recently, several studies have reported a short and strong H-bond known as CAHB with covalent bond-like properties (up to 48% strength)[41,42] that can form between favorably oriented and charged donor-acceptor pairs that have similar proton affinity or PZC ($|\Delta pK_a|$ or $|\Delta PZC| < \sim 5.0$, Supplementary Note 1)[43,44]. This short and strong H-bond has been shown to facilitate the stable immobilization of ionizable organic chemicals on various materials[44,45]. Therefore, CAHB could serve as the dominant driving force for stable laccase immobilization on Cellulose-DNA hydrogels given their $|\Delta PZC|$ value (0.39) (Supplementary Fig. 10). To test this, we measured the solution pH variation of laccase before and after immobilization on Cellulose-DNA hydrogels (Fig. 2a). The solution pH significantly and linearly increases with an increasing amount immobilized on the hydrogels, which is attributable to the gradual depletion of $H^+$ from the $H_2O$ upon CAHB formation (Fig. 2b)[37]. Additionally, a characteristic peak at 3809 cm$^{-1}$ occurs in the high-frequency region of the FTIR spectra and at 17.90 ppm in the very low-field region of $^1$HNMR spectra of the Cellulose-DNA hydrogels after laccase immobilization (Fig. 2c, d). These findings strongly suggest CAHB formation[46,47]. Notably, these potential CAHB peaks disappear upon replacing the solvent $H_2O$ with $D_2O$ (deuteration), again confirming that laccase was stably and abundantly immobilized on Cellulose-DNA hydrogels through CAHB. Importantly, the laccase immobilized on Cellulose-DNA hydrogels via CAHB exhibits significant comprehensive performance, outperforming the vast majority of immobilized laccase prepared via other approaches reported previously (Supplementary Fig. 11, Supplementary Table 4). In addition, comparable outcomes were observed for the immobilization of catalase (applied in textile industry, cosmetic therapy, etc., Supplementary Fig. 12) and lipase (utilized in plastic degradation, food manufacturing, etc., Supplementary Fig. 13) on the Cellulose-DNA hydrogels, demonstrating the versatility of CAHB as an effective strategy for enzyme immobilization. The immobilized amount (normalized by specific surface area) of the three enzymes on the Cellulose hydrogels (without DNA) decreased by 28.3-39.2% compared to that on the Cellulose-DNA hydrogels, which is primarily attributed to the fact that both C-OH and P-OH groups on the Cellulose-DNA hydrogels contribute to enzyme immobilization via CAHB (Supplementary Fig. 14).

To gain further understanding of the mechanisms of activity between laccase and Cellulose-DNA hydrogels at the molecular level, we conducted MD simulations to identify the specific binding sites responsible for CAHB formation. The simulation was performed for 100 ns, ensuring that the interaction between laccase and the

https://doi.org/10.1038/s41467-025-57720-x

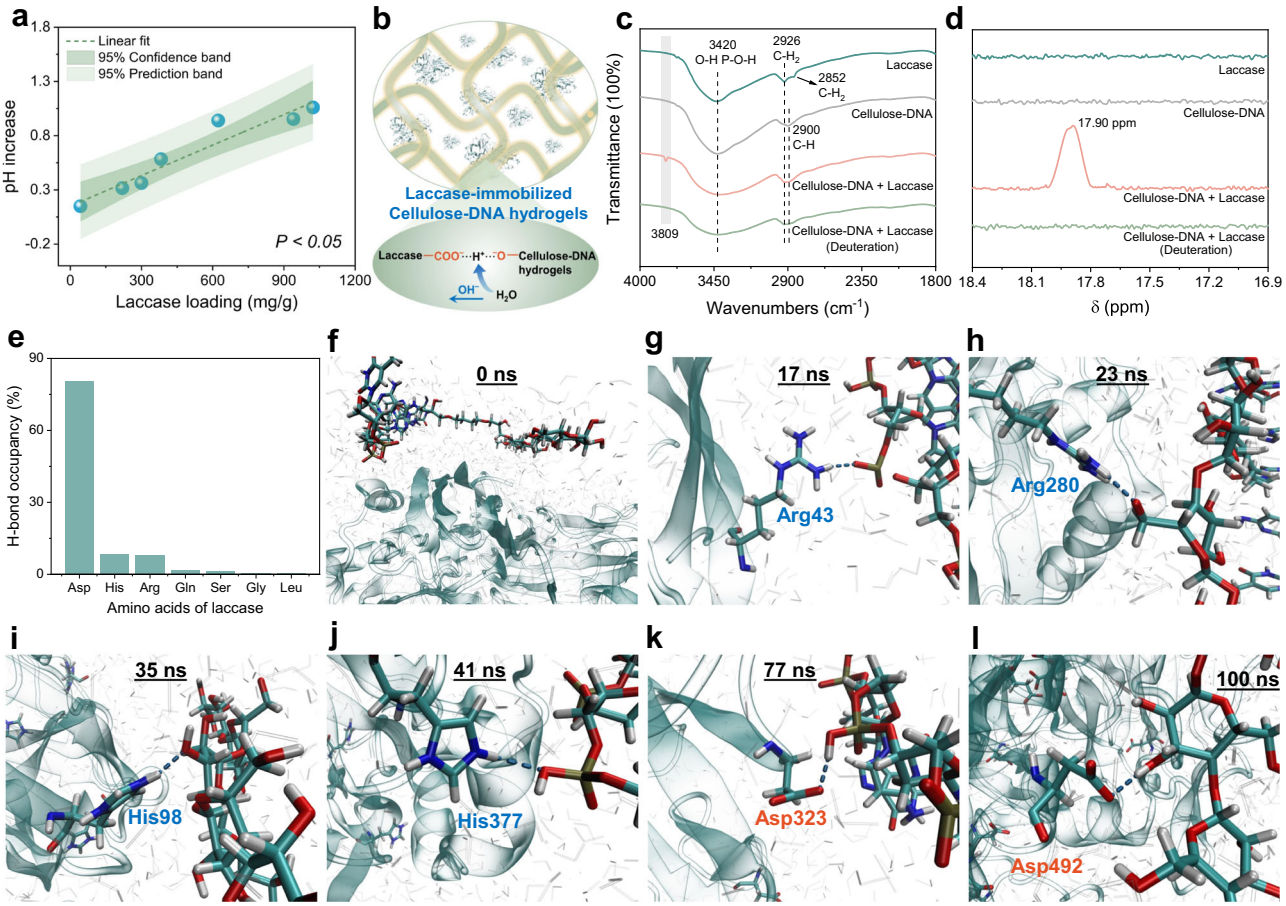


**Fig. 2 | CAHB mechanism of laccase immobilization on Cellulose-DNA hydrogels. a** Correlation between the amount of laccase immobilized on Cellulose-DNA hydrogels and solution pH changes before and after laccase immobilization. **b** Illustration of the suggested CAHB interaction between laccase and Cellulose-DNA hydrogels. FTIR (**c**) and $^1$H NMR (**d**) spectra of laccase, Cellulose-DNA hydrogels, and laccase-immobilized Cellulose-DNA hydrogels (including deuteration). **e** Contribution from different amino acids to H-bond formation between laccase and Cellulose-DNA hydrogels in 100 ns MD simulations. Initial state (**f**, 0 ns), 17 ns (**g**), 23 ns (**h**), 35 ns (**i**), 41 ns (**j**), 77 ns (**k**), and the final equilibrium state (**l**, 100 ns) of the H-bond interaction between Cellulose-DNA hydrogels and laccase by MD simulations. The gray wireframe molecular structure is the water molecule. Application of the CAHB strategy for enzyme immobilization is conditional (i.e., $|\Delta pK_a|$ or $|\Delta PZC|$ <-5.0). Both purified and impure enzymes can theoretically be used, as long as the enzyme surface exposes functional groups that can meet the requirements for CAHB formation. In practical applications, it may be necessary to balance the cost and contaminant treatment efficiency of the final product, depending on the specific context and requirements. In (**a**), data are presented as mean from three replicates ($n = 3$).

Cellulose-DNA hydrogels had reached equilibrium (Supplementary Fig. 15). Figure 2e illustrates the contributions from individual amino acids in laccase towards H-bond formation. Aspartic acid (Asp) overwhelmingly contributed 80.37%, which is 4.1-fold the sum of all other amino acids, including histidine (His, 8.36%), arginine (Arg, 7.17%), glutamine (Glu, 1.51%), serine (Ser, 1.18%), glycine (Gly, 0.46%) and leucine (Leu, 0.41%). A significant contribution from Asp can be attributed to the formation of strong CAHB (laccase–$COO^-$···$H^+$···$^-$OP/C–hydrogels) between the carboxylic groups (–COOH) on Asp and the oxygen-containing hydroxyl groups (C-OH, P-OH) on Cellulose-DNA hydrogels due to a small |ΔPZC| between them (1.00, Supplementary Fig. 16a–c). Weak ordinary H-bonds formed between Cellulose-DNA hydrogels and the –NH groups on His and Arg contributed little to their overall H-bond interactions with laccase due to high |ΔPZC| (8.99 and 8.30, Supplementary Fig. 16d–i). We further identified the dynamics of the representative conformations of H-bond interactions between Asp/His/Arg and P-OH/C-OH groups on Cellulose-DNA hydrogels within 100 ns simulation. At 17 ns and 23 ns, the –NH group on Arg formed H-bonds with P-OH and C-OH groups on Cellulose-DNA hydrogels, respectively (Fig. 2f–h); at 35 ns and 41 ns, the –NH group on His formed H-bonds with their C-OH and P-OH groups, respectively (Fig. 2i, j). These H-bonds are relatively weak. Subsequently, strong CAHB between the –COOH group on Asp and P-OH group on Cellulose-DNA hydrogels was established at 77 ns, and finally, laccase stably bound to C-OH groups on Cellulose-DNA hydrogels through strong CAHB was evident at the final equilibrium state of 100 ns (Fig. 2k, l). In addition, uncharged neutral amino acids, including glutamine, serine, glycine and leucine, theoretically formed ordinary H-bonds with Cellulose-DNA hydrogels, which also contributed little to the overall H-bond interactions with laccase[43].

To quantitatively evaluate the strength and stability of different H-bond conformations obtained by MD simulation, DFT calculations were performed. The CAHB (bond energy: ≤ -111.51 kJ/mol; bond length: ≤ 2.489 Å; and bond angle: ≥ 178.98°) formed between Asp and Cellulose-DNA hydrogels is clearly stronger than ordinary H-bonds (bond energy: ≥ -26.69 kJ/mol; bond length: ≥ 2.722 Å; and bond angle: ≤ 171.39°) that formed between His/Arg and Cellulose-DNA hydrogels (Fig. 3a–i, Supplementary Fig. 17). In addition, the CAHB ( ≥ 4.29 eV) exhibits a greater $E_{gap}$ value than the ordinary H-bond (≤ 3.56 eV) (Fig. 3j), indicating greater stability. Based on these experimental and computational findings, we conclude that Cellulose-DNA hydrogels primarily form strong and stable CAHB with Asp from laccase, which ensures efficient enzyme immobilization, activity and stability. The simulation results also have potential applicability for bioreactor design and programmable enzyme modification.

https://doi.org/10.1038/s41467-025-57720-x

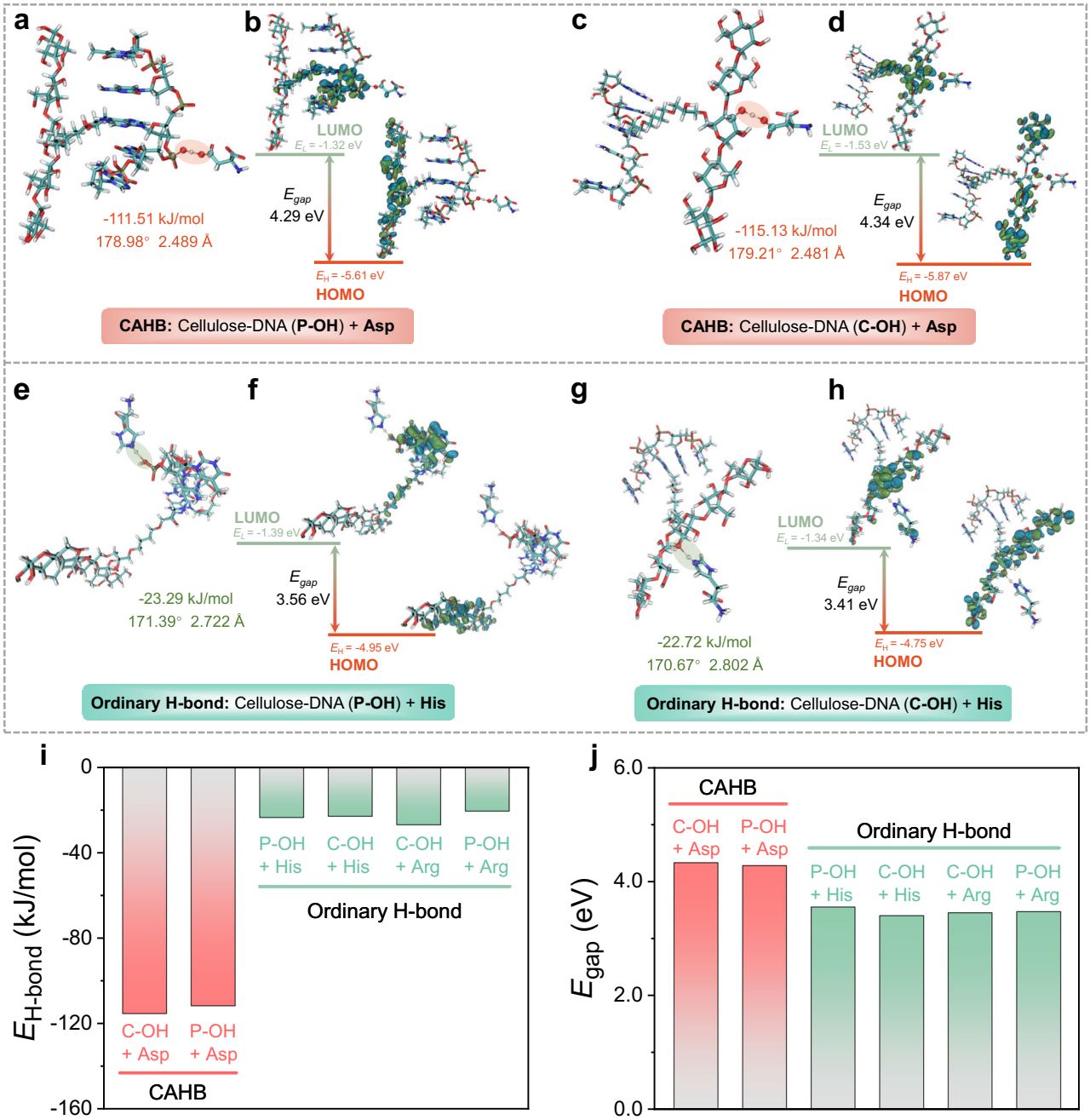


**Fig. 3 | Strength and stability of different H-bond configurations (from MD simulation) via DFT calculations.** Strength ($E_{H\text{-bond}}$, kJ/mol), bond length (Å), bond angle (°) and stability ($E_{gap}$, eV) of the H-bond between Asp from laccase and P-OH (**a**, **b**) or C-OH (**c**, **d**) from Cellulose-DNA hydrogels quantified through DFT calculations. A stronger H-bond can be attributed to a shorter bond length, accompanied with a larger bond angle and higher bond energy. Strength, bond length, bond angle and stability of the H-bond between His from laccase and P-OH (**e**, **f**) or C-OH (**g**, **h**) from Cellulose-DNA hydrogels quantified through DFT calculations. Strength (**i**) and stability (**j**) of the H-bond between Asp/His/Arg from laccase and P-OH or C-OH group from Cellulose-DNA hydrogels quantified through DFT calculations. The relevant data are presented in Supplementary Table 5. The "bond energy, bond length and bond angle" of CAHB formed between Asp from laccase and P-OH and C-OH groups from Cellulose-DNA hydrogels are "−111.51 kJ/mol, 2.489 Å, 178.98°" and "-115.13 kJ/mol, 2.481 Å, 179.21°", respectively. The corresponding values for the ordinary H-bonds formed between His and their P-OH and C-OH groups are "-23.29 kJ/mol, 2.722 Å, 171.39°" and "-22.72 kJ/mol, 2.802 Å, 170.67°", respectively. Similarly, the corresponding values for the ordinary H-bonds formed between Arg and their C-OH and P-OH groups are "−26.69 kJ/mol, 2.828 Å, 170.58°" and "-20.29 kJ/mol, 2.810 Å, 169.99°", respectively.

## Micropollutant removal by laccase-immobilized hydrogels

The contaminant removal performance of laccase-immobilized Cellulose-DNA hydrogels was evaluated using three representative micropollutants (Flu, 1-MFlu, 3-NFlu). These micropollutants have been widely detected in numerous aquatic environments and pose a significant risk to human health due to their carcinogenic, neurotoxic, and reproductive toxicity[48,49]. The total removal efficiency (the sum of sorption and degradation, > 93.5%) and net degradation efficiency (> 46.7%) of three micropollutants by the laccase-immobilized Cellulose-DNA hydrogels was 2.45-9.13 times that of the free laccase control (<23.8%) (Fig. 4a). The degradation rate of Flu (0.36 μg/h), 1-MFlu (0.38 μg/h) and 3-NFlu (0.30 μg/h) by the laccase-immobilized hydrogels during 0-4 h (reaching equilibrium) was 16.85-fold (Flu), 10.38-fold (1-MFlu), and 14.84-fold (3-NFlu) that achieved by free laccase, respectively (Fig. 4b). This

https://doi.org/10.1038/s41467-025-57720-x

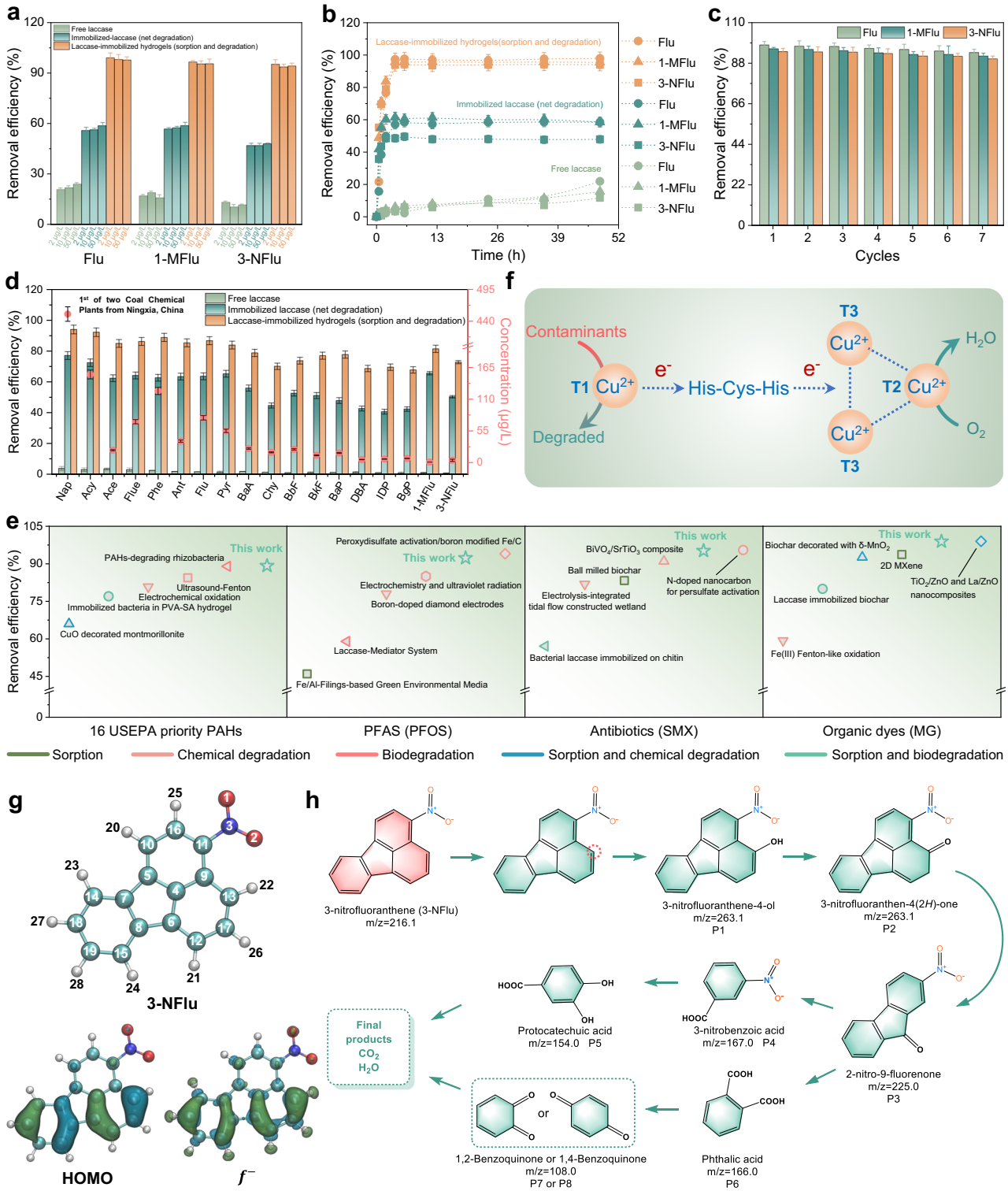


significantly greater activity at the early timepoints can be attributed to the capture of these three micropollutants. Importantly, the laccase-immobilized Cellulose-DNA hydrogels exhibited significant total removal efficiency (> 90.2%, Fig. 4c) and net degradation efficiency (> 46.2%, Supplementary Fig. 18) after undergoing 7 cycles, along with excellent long-term operational performance (30 days, Supplementary Fig. 19), highlighting the robustness of design. In addition, this hydrogel demonstrated impressive total removal efficiency (>92.3%) and net degradation efficiency (> 58.2%) towards PFAS (pentadecafluorooctanoic acid: PFOA, perfluorooctanesulfonic acid: PFOS, using the mediator 1-hydroxybenzotriazole), antibiotics (sulfamethoxazole: SMX, ciprofloxacin: CIP, using the mediator 1-hydroxybenzotriazole) and organic dyes (malachite green: MG, congo red: CR), demonstrating the significant potential of this strategy for addressing a wide range of emerging organic pollutants (Supplementary Fig. 20).

The environmental applicability of the laccase-immobilized hydrogels for removal of several micropollutants under a range of environmental conditions was further evaluated (Supplementary Figs. 21-22). Importantly, hydrogel performance was not significantly inhibited (<6.1%) under harsh conditions, including at pH 4.0-9.0 and

**Fig. 4 | Micropollutant removal by laccase-immobilized Cellulose-DNA hydrogels. a** Removal efficiency of micropollutants (Flu, 1-MFlu, 3-NFlu) at 2, 10, 50 μg/L by laccase-immobilized Cellulose-DNA hydrogels (the sum of sorption and degradation), immobilized laccase (net degradation), and free laccase. **b** Removal kinetics of three micropollutants at 50 μg/L by laccase-immobilized Cellulose-DNA hydrogels (the sum of sorption and degradation), immobilized laccase (net degradation), and free laccase. **c** Reusability of laccase-immobilized Cellulose-DNA hydrogels for three micropollutants removal at 50 μg/L over 7 cycles. **d** Removal efficiency of 16 USEPA priority PAHs, 1-MFlu and 3-NFlu in the first of two Coal Chemical Plant wastewater samples collected from Ningxia, China, by laccase-immobilized Cellulose-DNA hydrogels (the sum of sorption and degradation), immobilized laccase (net degradation), and free laccase, as well as their measured concentrations. **e** Comparison of removal performance of 16 USEPA priority PAHs in authentic wastewater, PFAS (e.g., perfluorooctanesulfonic acid: PFOS), antibiotics (e.g., sulfamethoxazole: SMX) and organic dyes (malachite green: MG) by the laccase-immobilized Cellulose-DNA hydrogels (sorption and biodegradation) in this work and other materials or approaches in previous reports. The relevant references and data are listed in Supplementary Table 8. **f** Degradation mechanism of micropollutants by immobilized laccase. Specifically, micropollutants underwent oxidation near the T1 copper center of laccase, leading to electron release; subsequently, these electrons were transferred through a tripeptide pathway consisting of Histidine-Cysteine-Histidine (His-Cys-His) to a trinuclear copper cluster site; finally, $O_2$ molecules in proximity to the trinuclear copper cluster site accepted these electrons, resulting in their reduction to $H_2O$. The sites where contaminants are most readily attacked and degraded are those most likely to lose electrons. **g** 3-NFlu molecular structure with labeled atomic positions, the HOMO of Flu, and the distribution of electrophilic ($f_A^-$) attacking sites based on the compressed Fukui function (CFF). A greater $f_A^-$ value and the more HOMO distribution indicate a greater likelihood of losing electrons. **h** Proposed degradation pathways of 3-NFlu by immobilized laccase. In (**a**–**d**), data are presented as mean ± S.D. from three replicates ($n = 3$); the dosage of free laccase was equivalent to the immobilized amount of laccase on the Cellulose-DNA hydrogels.

in the presence of a range of coexisting anions/cations, heavy metals, other organic contaminants, or DOM. Conversely, the corresponding inhibition imposed on free laccase under these conditions was as high as 21.2% (Supplementary Fig. 23). Last, the performance of the laccase-immobilized hydrogels and free laccase towards 16 USEPA priority PAHs, along with the two substituted PAHs 1-MFlu and 3-NFlu, in authentic wastewater from three Coal Chemical Plants (Ningxia and Shaanxi, China) was evaluated (Fig. 4d, Supplementary Fig. 24, Supplementary Table 6). The removal efficiency of free laccase consistently remained below 3.89%, which is likely a function of the enzyme's susceptibility to inactivation within the complex wastewater environment (Supplementary Table 7). Conversely, the total removal efficiency (66.2-95.4%) and net degradation efficiency (40.7-77.2%) achieved by the laccase-immobilized hydrogels were 22.3-93.0- and 17.5-64.3 times that of free laccase, respectively. Importantly, this level of performance surpasses that of the majority of other reported methods (including advanced oxidation processes, sorption, etc.) and materials (including sorbents and chemical catalysts, etc.) used for remediation (Fig. 4e, Supplementary Table 8). These observations underscore the high environmental applicability (robustness) of laccase immobilized on Cellulose-DNA hydrogels, and in particular, the importance of CAHB to enhancing their stability (Supplementary Fig. 25), activity and mechanical strength.

The potential degradation mechanisms of three representative micropollutants by the immobilized laccase were investigated by DFT calculations and gas chromatography-mass spectrometry. Based on previous work[50], laccase degraded contaminants via a single electron redox process (Fig. 4f). Given that C13 of 3-NFlu exhibited the highest Fukui electrophilic ($f_A^-$) index (0.0966) along with abundant HOMO (Fig. 4g, Supplementary Table 9), its degradation pathway was proposed based on the identified degraded products (Fig. 4h, Supplementary Fig. 26). Specifically, 3-NFlu was first converted to 3-nitrofluoranthene-4-ol, then to 3-nitrofluoranthen-4(*2H*)-one by tautomerization. The intermediate product 3-nitrofluoranthen-4(*2H*)-one underwent ring-opening and was converted to 2-nitro-9-fluorenone, then to 3-nitrobenzoic acid and phthalic acid. Subsequently, 3-nitrobenzoic acid and phthalic acid were converted to protocatechuic acid and 1,2-benzoquinone or 1,4-benzoquinone via oxidation and tautomerism processes, respectively, and the resulting intermediate was finally mineralized to $H_2O$ and $CO_2$. The degradation pathways for Flu (Supplementary Figs. 27, 28 and Supplementary Table 10) and 1-MFlu (Supplementary Figs. 29, 30 and Supplementary Table 11) are similar to those of 3-NFlu as they are congeners.

To further investigate the removal and degradation mechanisms of other pollutants (e.g., phenolic compounds), we conducted catechol elimination experiments, given that some studies suggest that the treatment of phenolic pollutants by laccase may lead to catalytic polymerization rather than complete degradation to $CO_2$ and $H_2O$[51,52]. Our results confirm this phenomenon, as phenolic pollutants (e.g., catechol) can be degraded and catalytically polymerized to valuable phenolic polymers (e.g., dimers and trimers) by laccase-immobilized hydrogels (Supplementary Fig. 31), offering a potential pathway for resource recovery of these contaminants in wastewater treatment.

To evaluate the environmental friendliness and economic feasibility of laccase-immobilized hydrogels for practical application, toxicity and bioconcentration factors of the degraded products, biocompatibility of the laccase-immobilized hydrogels, the costs of large-scale synthesis and remediation were assessed. The degraded products of the above three representative micropollutants demonstrated lower acute toxicity (i.e., *Daphnia magna* -$Log_{10}^{(48\ h\ LC50)}$) and bioconcentration levels than the corresponding parent compounds (Supplementary Fig. 32), indicating a reduction in the ecological toxicity of the pollutants. In addition, the laccase-immobilized Cellulose-DNA hydrogels showed no significant toxicity (24 and 48 h) to L929 mouse fibroblast cells at 1-10 mg/mL (Supplementary Fig. 33), indicating they possess suitable biocompatibility and environmental friendliness. Importantly, the plant-gate levelized cost of synthesizing 1 ton of laccase-immobilized hydrogels is approximately 2.11–1135 times lower than that of previously reported immobilized laccase (Supplementary Fig. 34a, b, Supplementary Tables 12-14, Supplementary Note 2). To remediate 1 ton of wastewater containing 50 μg/L 3-NFlu (with a removal efficiency > 90%), the cost that uses the laccase-immobilized hydrogels is about 4.78 times lower than that of free laccase, and this advantage increases to 19.7 times after 7 cycles of reuse (treating 7 tons of wastewater) (Supplementary Fig. 34c, d). These results collectively demonstrate that the laccase-immobilized hydrogels offer excellent environmental sustainability and cost-effectiveness, with significant potential for large-scale applications.

## Discussion

In summary, Cellulose-DNA hydrogels with high enzyme loading/activity, excellent mechanical strength and cost-effectiveness were constructed through a simple structural control strategy. The hydrogels exhibited strong micropollutant affinity (i.e., capture) that facilitated subsequent degradation by the immobilized enzyme. Our work presents an effective approach for enzyme immobilization (CAHB) that imparts excellent tolerance to pH-, temperature-, and storage conditions, as well as a high degree of recyclability. Importantly, the CAHB not only optimized both enzymatic activity and loading capacity, but also demonstrated transferability to additional enzymes, including catalase and lipase. Notably, apart from the enzymes tested in this work, the CAHB strategy has a great potential to be extended to other enzymes or microorganisms specifically designed to degrade emerging recalcitrant contaminants, such as the recently discovered enzyme for depolymerizing plastics (wax worm saliva enzymes)[53] and the anaerobic microorganisms for defluorinating PFAS[12].

The laccase-immobilized Cellulose-DNA hydrogels demonstrated impressive performance in removal and degradation of micropollutants, including PFAS, antibiotics, organic dyes, parent and substituted PAHs. Notably, performance levels here exceed that of most of other reported methods or materials. Further evaluation using parent and substituted PAHs as examples indicates that the excellent removal and degradation performance by the laccase-immobilized Cellulose-DNA hydrogels was not significantly affected by complex matrices, including anions/cations, heavy metals, organic compounds, or DOM. Removal efficiency of these contaminants was 17.5-93.0 times that of the commercial free laccase in authentic wastewater. Importantly, the laccase-immobilized Cellulose-DNA hydrogels not only reduced the ecological toxicity and hazards of the pollutants but also demonstrated excellent biocompatibility and cost-effectiveness.

These findings provide a framework and design paradigm for advanced bioreactors to efficiently and sustainably remove contaminants from wastewater, and have far reaching implications for water remediation and re-use in agriculture, public health, and other sectors. Looking forward, future research could focus on the following areas: (1) exploring the co-immobilization of multiple enzymes to enhance performance through cascade catalysis and synergistic reactions, as well as related enzyme-mediator systems; (2) targeting programmable enzyme modifications to precisely construct advanced, high-performance enzyme-based catalysts for specific catalytic functions, potentially expanding application of the CAHB strategy beyond wastewater remediation to the areas such as drug delivery and biofuel cells; (3) investigating the integration with other advanced methods (e.g., advanced sorbents and oxidation techniques) and optimizing scalability for industrial applications, including further cost optimization and scale-up trials.

## Methods

### Materials

All the chemicals and materials in this study are of analytical grade or higher and were used directly without additional purification (Supplementary Note 3).

### Synthesis of Cellulose- and Cellulose-DNA hydrogels

The natural biopolymer cellulose (5 g) was dissolved in a solution (95 g) containing urea (12 wt%) and NaOH (7 wt%) at −12 °C[35]. The resulting cellulose solution (5 wt%) was then subjected to centrifugal degassing at 2900 x *g* for 15 min and was then transferred to a mold maintained at 60 °C for 5 h for hydrogel formation. The hydrogels were soaked in 75% ethanol for 6 h and subsequently rinsed with DI-water for 3 days to eliminate any residual impurities.

DNA (3.0 g) from salmon sperm and varying amounts (0-1.6 g) of the cross-linker 1,4-butanediol diglycidyl ether (BDE) were added to the cellulose solution (5 wt%) to enhance mechanical strength and increase specific surface area. These augmented hydrogels should exhibit increased enzyme loading, as well as enhanced micropollutants capture and degradation. The steps for preparing the DNA-assembled cellulose hydrogel (Cellulose-DNA) are consistent with those for the unamended gels. The characterization methods, including FESEM-EDS, FTIR, XRD, and XPS, to evaluate the physicochemical properties of Cellulose- and Cellulose-DNA hydrogels are described in Supplementary Note 4.

### Immobilization of laccase on Cellulose-DNA hydrogels

For laccase immobilization, 40 mg of hydrogel was added to the phosphate buffer solution ($KH_2PO_4$, pH 6.0, 40 mL) that contained varying concentrations of laccase (0-2.5 mg/mL) (Supplementary Table 15). The resulting mixture was shaken in the dark at 180 rpm and 25 °C for 12 h. A preliminary investigation indicated that this time was sufficient to achieve equilibrium for laccase immobilization (Supplementary Fig. 35). After centrifugation at 2900 x g for 15 min, the supernatant was collected and the laccase content was determined using the Bradford method (Supplementary Note 5, Supplementary Fig. 36). The laccase immobilized hydrogels were rigorously washed with phosphate buffer solution and stored in a refrigerator at 4 °C for later use. The enzymatic activity of laccase in both free and immobilized states was determined using the ABTS method (Supplementary Note 6); the dose of the free laccase was equal to the amount of laccase immobilized on the Cellulose-DNA hydrogels. In addition, the pH and temperature, reusability, storage and immobilization stability of the laccase-immobilized Cellulose-DNA hydrogels were evaluated (Supplementary Note 7). Additional characterization methods, including NMR, FTIR, and CLSM, for the laccase immobilization mechanisms are detailed in Supplementary Note 8.

### Pollutant removal

The removal of three representative pollutants (fluoranthene: Flu, 1-Methylfluoranthene: 1-MFlu, 3-Nitrofluoranthene: 3-NFlu) at environmentally relevant concentrations (2-50 μg/L) by free laccase and laccase-immobilized Cellulose-DNA hydrogels was evaluated in 15 mL glass vials (see details in Supplementary Note 9 and Supplementary Fig. 37). To quantify the net pollutant degradation efficiency by immobilized laccase, Cellulose-DNA hydrogels or Cellulose-DNA hydrogels with inactivated laccase-immobilized (sorption) can be considered as a control to subtract its removal by laccase-immobilized Cellulose-DNA hydrogels (sorption and degradation) that is contributed from sorption. Our preliminary test showed different sorption strength of a given pollutant by Cellulose-DNA hydrogels and Cellulose-DNA hydrogels with inactivated laccase-immobilized, which could be that the enzyme denaturation process after immobilization may affect both the structural integrity and sorption sites of the hydrogels. Hence, the net degradation efficiency of pollutants was calculated using Cellulose-DNA hydrogels as a control (only sorption) in this study. To ensure a fair comparison between the pollutant removal efficiency of laccase-immobilized hydrogels and free laccase, the dose of the free laccase was equivalent to the amount of laccase immobilized on the Cellulose-DNA hydrogels. In addition, 7-cycle tests for pollutant removal by laccase-immobilized Cellulose-DNA hydrogels were conducted to assess reusability. Moreover, to explore scalability of the laccase-immobilized Cellulose-DNA hydrogels for pollutant removal, the tests were expanded to include additional contaminants beyond the three representative micropollutants (Flu, 3-NFlu, 1-MFlu); these tested pollutants included PFAS (pentadecafluorooctanoic acid: PFOA, perfluorooctanesulfonic acid: PFOS), antibiotics (sulfamethoxazole: SMX, ciprofloxacin: CIP) and organic dyes (malachite green: MG, congo red: CR) (Supplementary Note 9). In addition, removal of the 16 USEPA priority PAHs (including Flu) and the two substituted PAHs (1-MFlu, 3-NFlu) from authentic wastewater collected from three Coal Chemical Plants in Ningxia and Shaanxi, China was also tested (Supplementary Note 9 and Supplementary Fig. 38). The analytical methods for determining the analyte concentrations of the above pollutants and their degraded intermediate products are described in Supplementary Notes 10,11.

### Molecular dynamics simulation and density functional theory calculations

Molecular dynamics (MD) simulation was performed using GROMACS 2020.6 to investigate the H-bond sites between laccase and the Cellulose-DNA hydrogel[54]. The strength and stability of the representative H-bond conformations obtained from MD simulation were calculated by density functional theory (DFT) using the Gaussian 16 software package[55]. In addition, sorption energy ($E_{sorp}$) of the micropollutants and the energy gap ($E_{gap}$) of the Cellulose- and Cellulose-DNA hydrogels were determined by DFT calculation. The degradation of micropollutants was analyzed using the highest occupied molecular orbital (HOMO) and condensed Fukui functions to isolate the attacking sites determined by DFT calculations. The

methodological details for the MD simulation and associated DFT calculations are described in Supplementary Notes 12, 13 and Supplementary Fig. 39.

## Data availability

The authors declare that the data supporting the findings of this study are available within the paper and its Supplementary Information files. All data are available from the corresponding author upon request. Source data are provided with this paper.

## References


1. Grafton, Q., Biswas, A. K. & Tortajada, C. Signing up to safe water for billions. *Nature* **548**, 393–393 (2017).
2. Sadoff, C. W., Borgomeo, E. & Uhlenbrook, S. Rethinking water for SDG 6. *Nat. Sustain.* **3**, 346–347 (2020).
3. Sachs, J. D. et al. Six transformations to achieve the sustainable development goals. *Nat. Sustain.* **2**, 805–814 (2019).
4. Mekonnen, M. M. & Hoekstra, A. Y. Four billion people facing severe water scarcity. *Sci. Adv.* **2**, e1500323 (2016).
5. Liu, L. et al. The importance of system configuration for distributed direct potable water reuse. *Nat. Sustain.* **3**, 548–555 (2020).
6. Gokhale, D., Hamelberg, A. F. & Doyle, P. S. Multifunctional zwitterionic hydrogels for the rapid elimination of organic and inorganic micropollutants from water. *Nat. Water* **2**, 62–71 (2024).
7. Schwarzenbach, R. P. et al. The challenge of micropollutants in aquatic systems. *Science* **313**, 1072–1077 (2006).
8. Alsbaiee, A. et al. Rapid removal of organic micropollutants from water by a porous β-cyclodextrin polymer. *Nature* **529**, 190–194 (2016).
9. Liu, T. et al. Covalent organic framework membrane for efficient removal of emerging trace organic contaminants from water. *Nat. Water* **1**, 1059–1067 (2023).
10. Yang, Y. et al. Which micropollutants in water environments deserve more attention globally? *Environ. Sci. Technol.* **56**, 13–29 (2022).
11. Demissie, H. et al. Advances in micro interfacial phenomena of adsorptive micellar flocculation: Principles and application for water treatment. *Water Res.* **202**, 117414 (2021).
12. Jin, B. et al. Substantial defluorination of polychlorofluorocarboxylic acids triggered by anaerobic microbial hydrolytic dechlorination. *Nat. Water* **1**, 451–461 (2023).
13. Chen, Z. et al. Deglycosylation inactivation initiated by a novel periplasmic dehydrogenase complex provides a novel strategy for eliminating the recalcitrant antibiotic kanamycin. *Environ. Sci. Technol.* **57**, 4298–4307 (2023).
14. Sheldon, R. A., Basso, A. & Brady, D. New frontiers in enzyme immobilisation: Robust biocatalysts for a circular bio-based economy. *Chem. Soc. Rev.* **50**, 5850–5862 (2021).
15. Bolivar, J. M., Woodley, J. M. & Fernandez-Lafuente, R. Is enzyme immobilization a mature discipline? Some critical considerations to capitalize on the benefits of immobilization. *Chem. Soc. Rev.* **51**, 6251–6290 (2022).
16. Chen, W., Mo, J., Du, X., Zhang, Z. & Zhang, W. Biomimetic dynamic membrane for aquatic dye removal. *Water Res* **151**, 243–251 (2019).
17. Pei, X. et al. Putting precision and elegance in enzyme immobilisation with bio-orthogonal chemistry. *Chem. Soc. Rev.* **51**, 7281–7304 (2022).
18. Anwar, A., Imran, M. & Iqbal, H. M. N. Smart chemistry and applied perceptions of enzyme-coupled nano-engineered assemblies to meet future biocatalytic challenges. *Coord. Chem. Rev.* **493**, 215329 (2023).
19. Huang, W., Zhang, W., Gan, Y., Yang, J. & Zhang, S. Laccase immobilization with metal-organic frameworks: Current status, remaining challenges and future perspectives. *Crit. Rev. Environ. Sci. Technol.* **52**, 1282–1324 (2022).
20. Wang, X. & Wang, Q. Enzyme-laden bioactive hydrogel for biocatalytic monitoring and regulation. *Acc. Chem. Res.* **54**, 1274–1287 (2021).
21. Lou, J. & Mooney, D. J. Chemical strategies to engineer hydrogels for cell culture. *Nat. Rev. Chem.* **6**, 726–744 (2022).
22. Ott, W., Ceccarelli, A., Manning, J., Turner, N. J. & Oppenheimer, R. Data-driven enzyme immobilisation: A case study using DNA to immobilise galactose oxidase. *Eng. Biol.* **4**, 43–46 (2020).
23. Fu, J., Liu, M., Liu, Y., Woodbury, N. W. & Yan, H. Interenzyme substrate diffusion for an enzyme cascade organized on spatially addressable DNA nanostructures. *J. Am. Chem. Soc.* **134**, 5516–5519 (2012).
24. Ahmadian, M. & Jaymand, M. Interpenetrating polymer network hydrogels for removal of synthetic dyes: A comprehensive review. *Coord. Chem. Rev.* **486**, 215152 (2023).
25. Rodrigues, R. C., Berenguer-Murcia, Á., Carballares, D., Morellon-Sterling, R. & Fernandez-Lafuente, R. Stabilization of enzymes via immobilization: Multipoint covalent attachment and other stabilization strategies. *Biotechnol. Adv.* **52**, 107821 (2021).
26. Weerasundara, L., Gabriele, B., Figoli, A., Ok, Y. S. & Bundschuh, J. Hydrogels: Novel materials for contaminant removal in water-a review. *Crit. Rev. Environ. Sci. Technol.* **51**, 1970–2014 (2020).
27. Chen, Q. et al. Active and stable alcohol dehydrogenase-assembled hydrogels via synergistic bridging of triazoles and metal ions. *Nat. Commun.* **14**, 2117 (2023).
28. Zhou, W., Zhang, W. & Cai, Y. Laccase immobilization for water purification: A comprehensive review. *Chem. Eng. J.* **403**, 126272 (2021).
29. Han, Y., Han, L., Yao, Y., Li, Y. & Liu, X. Key factors in FTIR spectroscopic analysis of DNA: The sampling technique, pretreatment temperature and sample concentration. *Anal. Methods* **10**, 2436–2443 (2018).
30. Jangir, D. K., Tyagi, G., Mehrotra, R. & Kundu, S. Carboplatin interaction with calf-thymus DNA: A FTIR spectroscopic approach. *J. Mol. Struct.* **969**, 126–129 (2010).
31. Kang, K. et al. Preparation of carbon quantum dots from ionic liquid modified biomass for the detection of $Fe^{3+}$ and $Pd^{2+}$ in environmental water. *Ecotoxicol. Environ. Saf.* **255**, 114795 (2023).
32. Li, Z. et al. Sustainable, flexible, and superhydrophobic functionalized cellulose aerogel for selective and versatile oil/water separation. *ACS Sustain. Chem. Eng.* **7**, 9984–9994 (2019).
33. Wittmar, J. et al. What does ectoine do to DNA? A molecular-scale picture of compatible solute-biopolymer interactions. *J. Phys. Chem. B.* **124**, 7999–8011 (2020).
34. Cîrcu, M., Nan, A., Borodi, G., Liebscher, J. & Turcu, R. Refinement of magnetite nanoparticles by coating with organic stabilizers. *Nanomaterials* **6**, 228 (2016).
35. Wang, S. et al. Strong, tough, ionic conductive, and freezing-tolerant all-natural hydrogel enabled by cellulose-bentonite coordination interactions. *Nat. Commun.* **13**, 3408 (2022).
36. Yoosefian, M., Ansarinik, Z. & Etminan, N. Density functional theory computational study on solvent effect, molecular conformations, energies and intramolecular hydrogen bond strength in different possible nano-conformers of acetaminophen. *J. Mol. Liq.* **213**, 115–121 (2016).
37. Zhang, J. et al. Direct spectroscopic evidence for charge-assisted hydrogen-bond formation between ionizable organic chemicals and carbonaceous materials. *Environ. Sci. Technol.* **56**, 9356–9366 (2022).
38. Zhu, Y. et al. Continuous artificial synthesis of glucose precursor using enzyme-immobilized microfluidic reactors. *Nat. Commun.* **10**, 4049 (2019).
39. Feng, D. et al. Stable metal-organic frameworks containing single-molecule traps for enzyme encapsulation. *Nat. Commun.* **6**, 5979 (2015).

40. Vázquez-González, M., Wang, C. & Willner, I. Biocatalytic cascades operating on macromolecular scaffolds and in confined environments. *Nat. Catal.* **3**, 256–273 (2020).
41. Dereka, B. et al. Crossover from hydrogen to chemical bonding. *Science* **371**, 160–164 (2021).
42. Li, X., Pignatello, J. J., Wang, Y. & Xing, B. New insight into adsorption mechanism of ionizable compounds on carbon nanotubes. *Environ. Sci. Technol.* **47**, 8334–8341 (2013).
43. Gilli, P., Pretto, L., Bertolasi, V. & Gilli, G. Predicting hydrogen-bond strengths from acid-base molecular properties. The p$K_a$ slide rule: Toward the solution of a long-lasting problem. *Acc. Chem. Res.* **42**, 33–44 (2009).
44. Li, X., Gámiz, B., Wang, Y., Pignatello, J. J. & Xing, B. Competitive sorption used to probe strong hydrogen bonding sites for weak organic acids on carbon nanotubes. *Environ. Sci. Technol.* **49**, 1409–1417 (2015).
45. Ling, C. et al. High adsorption of sulfamethoxazole by an amine-modified polystyrene–divinylbenzene resin and its mechanistic insight. *Environ. Sci. Technol.* **50**, 10015–10023 (2016).
46. Sorgenfrei, N. et al. NMR spectroscopic characterization of charge assisted strong hydrogen bonds in brønsted acid catalysis. *J. Am. Chem. Soc.* **138**, 16345–16354 (2016).
47. Wang, Y. et al. Effects of charge-assisted hydrogen bond on sorption and co-sorption of pharmaceutical contaminants on carbonaceous materials: Spectroscopic and theoretical studies. *Sci. Total Environ.* **908**, 168375 (2024).
48. Han, M. et al. Sources of the elevating polycyclic aromatic hydrocarbon pollution in the western south China sea and its environmental implications. *Environ. Sci. Technol.* **57**, 20750–20760 (2023).
49. Peng, B., Dong, Q., Li, F., Wang, T., Qiu, X. & Zhu, T. A systematic review of polycyclic aromatic hydrocarbon derivatives: Occurrences, levels, biotransformation, exposure biomarkers, and toxicity. *Environ. Sci. Technol.* **57**, 15314–15335 (2023).
50. Song, Y. et al. Enhanced transformation of organic pollutants by mild oxidants in the presence of synthetic or natural redox mediators: A review. *Water Res.* **189**, 116667 (2021).
51. Llevot, A., Grau, E., Carlotti, S., Grelier, S. & Cramail, H. Selective laccase-catalyzed dimerization of phenolic compounds derived from lignin: Towards original symmetrical bio-based (bis) aromatic monomers. *J. Mol. Catal. B: Enzym.* **125**, 34–41 (2016).
52. Sun, X. et al. Laccase-catalyzed oxidative polymerization of phenolic compounds. *Appl. Biochem. Biotechnol.* **171**, 1673–1680 (2013).
53. Sanluis-Verdes, A. et al. Wax worm saliva and the enzymes therein are the key to polyethylene degradation by *Galleria mellonella*. *Nat. Commun.* **13**, 5568 (2022).
54. Abraham, M. J. et al. Gromacs: High performance molecular simulations through multi-level parallelism from laptops to supercomputers. *SoftwareX* **1-2**, 19–25 (2015).
55. Frisch, M. J. et al. Gaussian 16, Revision C.01. (Gaussian, Inc., Wallingford C.T, 2019).


## Acknowledgements

This study was supported by the National Natural Science Foundation of China (41821005, X.W and 41991312, X.W).

## Author contributions

J.Z. and X.W. conceptualized the study and wrote the original draft manuscript. J.Z., J.H., X.Y., C.Y., and L.D. conducted the experiments and analyzed the data. J.C.W., S.T., and X.W. revised the manuscript and made comments and edits to finalize the paper. All authors discussed the results and contributed to the writing of the manuscript.

## Competing interests

The authors declare no competing interests.

## Additional information

**Supplementary information** The online version contains supplementary material available at https://doi.org/10.1038/s41467-025-57720-x.

**Correspondence** and requests for materials should be addressed to Xilong Wang.

**Peer review information** *Nature Communications* thanks Dean Brady, who co-reviewed with Mudzuli MaphuphaAnming Wang, and Wenxiang Zhang for their contribution to the peer review of this work. A peer review file is available.